Determining preclinical safety of aclarubicin in pediatric malignancies

Tu, D.S.; Olson, A.K.; Waggie, K.S.; Garcia, N.M.; Hoglund, V.J.; Walter, S.I.; ... ; Ganapathi, S.S.

Pediatric Blood & Cancer

WILEY

Pediatric Blood & Cancer | SIOP INTERNATIONAL SOCIETY OF PAEDIATRIC ONCOLOGY | aspho The American Society of Pediatric Hematology/Oncology

RESEARCH ARTICLE OPEN ACCESS

Determining Preclinical Safety of Aclarubicin in Pediatric Malignancies

Darleen S. Tu[1] | Aaron K. Olson[2,3] | Kimberly S. Waggie[4] | Nicolas M. Garcia[1] | Virginia J. Hoglund[1] | Stephanie I. Walter[1] | Jenna R. Rosinski[1] | Harini Sadeeshkumar[1] | Radhika Patel[5] | Erolcan Sayar[5] | Michael C. Haffner[5] | Lisa Maves[3,6] | Jacques Neefjes[7] | Jay F. Sarthy[1,3] | Elizabeth R. Lawlor[1,3] | Shireen S. Ganapathi[1,3]

[1]Ben Towne Center for Childhood Cancer and Blood Disorders Research, Seattle Children's Research Institute, Seattle, Washington, USA | [2]Center for Integrative Brain Research, Seattle Children's Research Institute, Seattle, Washington, USA | [3]Department of Pediatrics, University of Washington, Seattle, Washington, USA | [4]Department of Comparative Medicine, University of Washington, Seattle, Washington, USA | [5]Division of Human Biology, Fred Hutchinson Cancer Research Center, Seattle, Washington, USA | [6]Center for Developmental Biology and Regenerative Medicine, Seattle Children's Research Institute, Seattle, Washington, USA | [7]Department of Cell and Chemical Biology, ONCODE Institute, Leiden University Medical Center, Leiden, the Netherlands

Correspondence: Elizabeth R. Lawlor (Beth.Lawlor@seattlechildrens.org) | Shireen S. Ganapathi (shireen.ganapathi@seattlechildrens.org)

Received: 15 May 2025 | **Revised:** 24 October 2025 | **Accepted:** 28 October 2025

Keywords: anthracyclines | cardiotoxicity | epigenetics | preclinical models

ABSTRACT

Background: Anthracyclines are among the most effective chemotherapeutic agents used to treat pediatric malignancies. However, their clinical use is limited by dose-dependent toxicities, particularly cardiotoxicity and secondary malignancies. Aclarubicin (Acla) is an anthracycline derivative that induces chromatin damage while sparing DNA damage, offering potential therapeutic benefit with reduced long-term toxicity.

Methods: We evaluated the anti-tumor efficacy and safety profile of Acla in multiple in vitro pediatric cancer models and in vivo mouse models designed to mimic anthracycline re-treatment following prior doxorubicin (Doxo) exposure. Tumor growth, genotoxic stress, survival, and organ toxicity were assessed.

Results: Acla demonstrated robust anti-tumor activity comparable to Doxo across diverse pediatric in vitro models. Unlike Doxo, Acla treatment did not induce significant genotoxic stress. In vivo, mice receiving Acla after Doxo exposure showed no evidence of cumulative cardiotoxicity or end-organ damage. In contrast, a second course of Doxo led to significant toxic mortality but was surprisingly not attributable to classic cardiac injury.

Conclusion: Our study highlights Acla as a promising anthracycline derivative for pediatric cancers, with potent anti-tumor efficacy and a superior safety profile, even following prior anthracycline exposure. These results support continued investigation of chromatin-damaging anthracyclines that can kill pediatric cancer cells without inducing genotoxic stress. In addition, our studies underscore the need to refine preclinical models to better understand both acute and chronic anthracycline toxicities in pediatric and adolescent populations.

Abbreviations: Acla, aclarubicin; ALT, alanine aminotransferase; AYA, adolescent and young adult; BL, Burkitt lymphoma; CBC, complete blood count; D–A/Doxo–Acla, doxorubicin–aclarubicin treatment group; D–D/Doxo–Doxo, doxorubicin–doxorubicin treatment group; Doxo, doxorubicin; Doxo–saline/D–S, doxorubicin–saline treatment group; dsDNA, DNA damage double-strand break; Echo, echocardiogram; EF, ejection fraction; EwS, Ewing sarcoma; FS, fractional shortening; HL, Hodgkin lymphoma; HR, heart rate; IF, immunofluorescence; IHC, immunohistochemistry; IP, intraperitoneal; LV, left ventricle; LYM, total lymphocyte count; OS, osteosarcoma; PLT, total platelet count; TLR-4, toll-like receptor 4; Topo II, topoisomerase II.

1 | Introduction

Anthracyclines remain one of the most important classes of chemotherapeutic agents used to treat pediatric and adolescent and young adult (AYA) malignancies. Nevertheless, although dose escalation of anthracyclines has improved survival, it is limited by dose-dependent toxicities, including infertility, secondary malignancies, and cardiotoxicity [1–4]. These dose-dependent toxicities on healthy tissue limit further use in upfront therapy or at relapse [4].

Anthracyclines function as topoisomerase II (topo II) poisons, inducing double-strand DNA breaks (dsDNA) and apoptosis [5]. Its ability to poison topo II leads to generation of free radicals, and targeted Topo IIβ poisoning in cardiomyocytes induces cardiac toxicity [4, 6, 7]. However, it was recently discovered that anthracyclines also cause chromatin damage by evicting histones, leading to epigenetic and transcriptional alterations and subsequent tumor cell death [8–11]. Unlike etoposide, which solely causes DNA damage [8], anthracyclines attenuate DNA repair through H2AX phosphorylation. Importantly, chromatin and DNA damage occur at separate genomic loci, indicating independent mechanisms [12]. Emerging evidence suggests that chromatin damage contributes to anti-tumor efficacy without driving off-target toxicity [12, 13].

Aclarubicin (Acla) is a chromatin-damaging anthracycline with minimal genotoxicity due to its distinct structure [12–14]. Acla has been used for decades in Europe, Japan, and China to treat elderly patients with acute myeloid leukemia (AML) due to its favorable toxicity profile [15–17]. Recent preclinical work demonstrated equivalent anti-tumor efficacy of Acla and doxorubicin (Doxo), whereas only high doses of Doxo-induced significant secondary off-target toxicities—cardiotoxicity and hematologic secondary malignancies [12, 13]. The biodistribution of Acla is different from Doxo, and Acla preferentially accumulates in hematopoietic organs such as thymus, spleen, and bone marrow [12]. With increasing recognition of chromatin-mediated anticancer effects in anthracyclines, Acla offers a promising strategy to preserve therapeutic efficacy while reducing long-term toxicities in pediatric and AYA malignancies.

Here, we evaluated the preclinical efficacy of Acla and Doxo across a panel of pediatric cancer cell lines and found comparable in vitro cytotoxicity, independent of genotoxic damage. Given that patients with relapsed disease often approach lifetime anthracycline limits, we modeled Acla administration following prior Doxo exposure. Although additional Doxo led to significant toxicity and premature mortality, Acla was well tolerated in pretreated C57BL/6J mice and did not induce significant organ dysfunction. These findings support the anti-tumor efficacy of Acla and the potential and feasibility of Acla in the relapsed pediatric cancer setting.

2 | Materials and Methods

2.1 | Cell Lines

CHLA10—Ewing sarcoma (EwS), L-428—Hodgkin lymphoma (HL), and Raji–Burkitt lymphoma (BL) cell lines were obtained from ATCC and COG cell line repositories (https://www.childrensoncologygroup.org/). CHLA10 was cultured in IMDM (Fisher) supplemented with 1% L-glutamine and 20% fetal bovine serum (FBS) and 1× insulin–transferrin–selenium–ethanolamine (Gibco). Raji and L-428 were cultured in RPMI 1640 (Gibco) with 10% FBS. OS833–Osteosarcoma (OS) cell linewas kindly gifted from the Sweet Cordero laboratory at UCSF. OS833 was cultured in DMEM (+glucose, +pyruvate, +glutamine) (Gibco 11995-065), 10% FBS, and 1% pen/strep. All cell lines were maintained in a humidified atmosphere of 5% CO_2 at 37°C. Regular *Mycoplasma* and short tandem repeat confirmation was performed.

2.2 | Western Blots

Cells were lysed with RIPA buffer (Fisher Scientific) supplemented with protease and phosphatase inhibitors (Sigma). Western blot was performed using the Bio-Rad Mini-PROTEAN Tetra System. Following transfer, nitrocellulose membranes were blocked in Odyssey Blocking Buffer (LI-COR) for 1 h. Membranes were washed and incubated rotating overnight at 4°C with a primary antibody. Membranes were then washed in TBST and incubated with a secondary antibody (LICOR IRDye 700CW or 800CW; 1:10,000) for 1 h. Membranes were imaged on a LI-COR Odyssey scanner.

2.3 | Cell Viability Assays

Cells were seeded at a density of 2000–5000 cells/well in 100 µL medium in 96-well plates. Serial dilutions of Acla (supplied by the Neefjes Laboratory, LUMC), Doxo (Millipore Sigma, Cat #353), and etoposide (MedChem Express, Cat#HY-13629) diluted in 100 µL media were added and incubated for 72 h. Cell viability was measured by adding 40 µL Cell-Titer Glo ATP-based assay (Promega). Luminescence was read using SpectraMax iD5 plate reader.

2.4 | Immunofluorescence (IF)

Cells were fixed with 4% PFA in PBS for 10 min, then washed with PBS. Cells were permeabilized for 10 min with 0.3% Triton-X and then blocked with 0.2% BSA in PBS for 1 h at room temperature. Cytospins were incubated with RAD51 (1:50, Sigma, Cat#ZRB1492) in antibody dilution buffer (Ventana Cat. ABD250) at 37°C in a humidified chamber, followed by secondary PV Poly-HRP Anti-Rabbit IgG (Leica Microsystems Cat. PV6119) for 30 min/37°C. Alexa Fluor 568 Tyramide (Invitrogen, B40956) was then used for RAD51 detection. Slides were counterstained with DAPI (Thermo Fisher Scientific) and mounted with Prolong (Thermo Fisher Scientific), and fluorescence images were captured using a Nikon Eclipse E800 microscope (Nikon). Fluorescent nuclear foci were visualized by microscopy and quantified using ImageJ.

2.5 | In Vivo Cardiotoxicity Experiments

All experimental procedures adhere to the *Guide for the Care and Use of Laboratory Animals* and were approved by Seattle

Children's Research Institute IACUC [18]. The institute is fully AAALAC-accredited and has a Public Health Service approved Animal Welfare Assurance. C57BL/6J (7-week-old) male mice were purchased from Jackson Laboratory (JAX #000664) and acclimated to study for 1 week. Doxo (Millipore Sigma, Cat#353) and Acla (provided by Neefjes Laboratory, LUMC) preparations were reconstituted with 0.9% sterile saline to a 0.5 mg/mL solution. Doxo and Acla were dosed at 5 mg/kg/dose intraperitoneal injections (IP) weekly. Details of dosing schedule are found in subsequent results and figure legends. Equivalent volume of saline was delivered to vehicle mice. Mice were monitored at least three times a week for early end-point criteria that included signs of morbidity or weight loss beyond 15% of starting body weight. All mice were humanely sacrificed by carbon dioxide asphyxiation at the end of study.

2.6 | Echocardiogram

Echocardiograms (echos) were performed by a cardiologist blinded to treatment groups and analysis, the methods of the echos are previously described [19, 20]. VEVO 3100 High-Resolution Micro-Ultrasound System (VisualSonics Inc., Toronto, Canada) and MX550D transducer were used for echo measurements under isoflurane anesthesia at a 3% induction concentration and a maintenance of 1% in 100% oxygen at a flow of 1 LPM. Mice were positioned supine, and ECG leads were placed for continuous monitoring during image acquisition. Heart rates (HRs) were maintained between 400 and 600 beats per minute, and heat support was provided to maintain body temperature at 37.0–37.5°C.

Hearts were measured in the parasternal short axis at the mid-papillary level of the left ventricle (LV) and taken in M-mode for end-diastole (EDD) and end-systole (ESD). Fractional shortening (FS) was calculated by [(LVEDD − LVESD)/LVEDD × 100] in a parasternal short axis view for at least three heart beats. An apical four-chamber view with pulsed Doppler was used to measure early diastolic *trans*-mitral flow velocity (MV E) and late diastolic *trans*-mitral flow velocity (MV A) along with the myocardial performance index, calculated by [isovolumic relaxation time + isovolumic contraction time)/aortic ejection time]. All other reported Echo functional measurements were calculated in Vevo LAB (version 5.6.1, VisualSonics Inc., Toronto, Canada). Measurements were performed on five mice from each group before the start of the second exposure and 12 weeks after the final exposure, or earlier if the mouse met criteria for humane euthanasia.

2.7 | In Vivo Serum Analysis

Prior to euthanasia, blood was collected awake by submental lancet puncture or via retroorbital bleeding under isoflurane anesthesia (2% maintenance). For complete blood counts (CBCs), two drops of blood were placed in EDTA-coated tubes and analyzed using ElementHt5 (Heska, Loveland, CO, USA). For additional serum analysis, blood was allowed to coagulate for 20–45 min and spun at 2500 RPM for 15 min. Isolated serum was frozen at −20°C and submitted to IDEXX (Sacramento, CA, USA).

2.8 | Tissue Preparation

Heart, lung, kidney, and liver were weighed, and tibial length was measured during tissue collection. The formula (organ weight ÷ tibial length) was used to index heart weights to normalize for mouse variation in body size [21]. Hearts were fixed in 10% neutral buffered formalin, and paraffin-embedded sections were cut to 2 µm thickness in a four-chamber view. Sections were stained with hematoxylin and eosin (H&E) to be evaluated for vacuolization and trichrome special stain to highlight fibrosis. A peroxidase-based detection system (B40925, Thermo Fischer) and ImmPact DAB Substrate Kit (SK-4105, Vector Laboratories) were used to perform immunohistochemistry (IHC) with periostin primary antibody (1:100, ab215199, Abcam) and Rabbit IgG (1:100, 02-6102, Invitrogen) as a negative control. Whole slides were scanned with ZIESS Axioscan 7 (White Plains, NY, USA), and histologic images were captured using QuPath (version 0.5.1).

2.9 | Histology Analysis

A veterinary pathologist blinded to treatment groups evaluated whole heart sections and scored ventricles by severity of vacuolization, fibrosis, and IHC stain uptake. The right ventricle, LV, and interventricular septum received a score and were summed for each heart. Scores were averaged by treatment group.

2.10 | Statistical Analysis

GraphPad Prism (version 10) was used for statistical analysis. Kaplan–Meier curves were analyzed using log-rank (Mantel-Cox) test. Student's *t*-test was used to determine significant differences between two groups and one-way ANOVA with Tukey's Multiple Comparison for any group analysis greater than two. Statistical significance is denoted as *p value of <0.05, **$p < 0.01$, ***$p < 0.001$, ****$p < 0.0001$ unless specified otherwise.

3 | Results

3.1 | Acla Has Equivalent In Vitro Efficacy to Doxo Without Inducing Genotoxic Damage

We first compared the anti-tumor efficacy of Acla and Doxo in vitro. A panel of pediatric cancer cell lines was selected for which Doxo is used in upfront standard of care. Specifically, we tested CHLA10 (EwS), OS833 (OS), L-428 (HL), and Raji (BL). Etoposide was incorporated in these viability assays as a topo II poison that generates DNA breaks but does not induce chromatin damage [8]. In all models, we observed comparable cytotoxicity between Acla and Doxo, with no statistically significant differences in sensitivity; however, there was a striking and statistically significant decrease in sensitivity to etoposide as compared to Acla and/or Doxo (Figure 1A). We next assessed the degree of DNA damage induced by Acla, Doxo, and etoposide at doses that induced a viability defect. All four cell lines (CHLA10, OS833, L-428, Raji) were exposed to 100 nM Acla, 100 nM Doxo, 250 nM etoposide, or vehicle for 48 h. Protein lysates were then assessed for accumulation of DNA damage, using γ-H2AX, a marker of DNA double-strand break repair. At

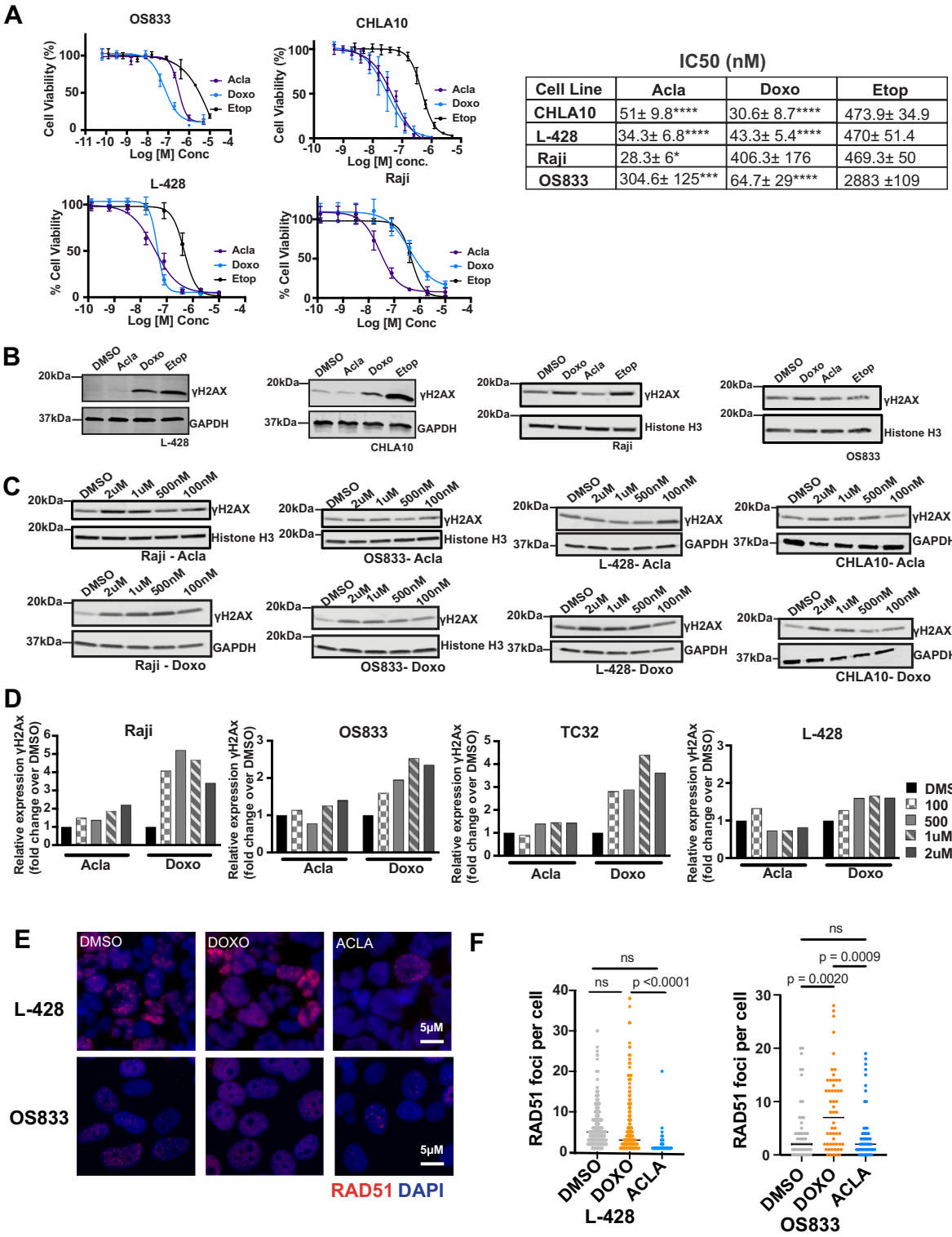

FIGURE 1 | Aclarubicin has equivalent in vitro efficacy to doxorubicin without inducing genotoxic damage. (A) Dose–response curves of OS833 (OS), CHLA10 (EwS), L-428 (HL), and Raji (BL). Cells were treated with serial dilutions of Acla, Doxo, and etoposide, or relevant DMSO controls. *Y*-axis represents % viability as compared to DMSO control. Graph is representative of at least two to three individual experiments with three technical replicates. Table shows IC50 values with standard error of mean. Statistical significance of efficacy between Doxo, Acla, and etoposide was determined by one-way ANOVA test. (*$p < 0.05$, **$p < 0.01$ ***$p < 0.001$, ****$p < 0.0001$). (B) Immunoblot of γ-H2AX protein expression (representative image of $n = 2$) of OS833 (OS), CHLA10 (EwS), L-428 (HL), and Raji (BL) cells treated with 100 nM aclarubicin, 100 nM doxorubicin, or 250 nM etoposide for 48 h. (C) Immunoblot of cells treated with 100 nM, 500 nM, 1 μM, or 2 μM of Acla or Doxo for 24 h. (D) Fold change of relative γ-H2AX expression (normalized to loading control) above DMSO. (E) DAPI and RAD51 staining of L-428 and OS833 cells treated with DMSO, 1 μM Doxo, or 1 μM Acla for 24 h (representation image of $n = 2$). (F) Quantification of RAD51 foci nuclear staining per cell. Statistical significance was calculated using one-way ANOVA (*$p < 0.05$, **$p < 0.01$, ***$p < 0.001$). Acla, aclarubicin; Doxo, doxorubicin; Etop, etoposide.

doses that induced a cytotoxic effect, only Doxo and etoposide induced a DNA damage response (Figure 1B). To determine if higher doses of Acla induced DNA damage, we exposed all four cell lines to escalating doses of either Acla or Doxo (100 nM, 500 nM, 1 μM, 2 μM) for 24 h and assessed γ-H2AX expression. We consistently observed that Doxo treatment was associated with high expression of γ-H2AX. In contrast, despite escalating doses of Acla, an increase in expression of γ-H2AX was not observed (Figure 1C,D). Finally, we assessed downstream activation of DNA damage response pathways in response to Doxo or Acla treatment through RAD51 IF, which localizes to sites of DNA damage. L-428 and OS833 cells were exposed to 1 μM of Acla, Doxo, or DMSO for 24 h. At baseline, both cell lines exhibited RAD51 nuclear staining. Upon Doxo treatment, RAD51 nuclear foci were significantly increased, consistent with induction of DNA damage. In contrast, Acla-treated cells showed RAD51 staining comparable to vehicle control (Figure 1E,F). This suggests that RAD51 is released from chromatin by Acla, similar to the mechanism observed for histones and other proteins. In summary, Acla shows cytotoxic efficacy comparable to Doxo but does not induce genotoxic damage, which is consistent with a primary mechanism of chromatin-mediated cytotoxicity.

3.2 | Modeling Doxo Cardiotoxicity In Vivo

There are multiple published mouse models for evaluating Doxo-induced cardiotoxicity using different mouse strains and dosing. Thus, we first sought to validate induction of Doxo-induced cardiotoxicity in the C57BL/6J strain. Recent studies inducing cardiotoxicity use a cumulative Doxo dose of 20–25 mg/kg and evaluate for cardiac changes by histology 1–13 weeks after the last dose of Doxo is delivered [22–24]. Given this, we exposed non-tumor bearing C57BL/6J mice to saline or 5 mg/kg Doxo weekly for total cumulative doses of 20, 25, or 30 mg/kg. Mice were observed for up to 13 weeks after the last dose of Doxo, at which point all animals were euthanized (Figure 2A). Echocardiograms were performed at baseline and at time of sacrifice (Figure 2A). Only two mice, one that received a total cumulative dose of 25 mg/kg and one that received 30 mg/kg, required humane euthanasia prior to endpoint due to weight loss >15% (Figure 2B). All mice that received Doxo had histologic evidence of cardiotoxicity demonstrated by increased vacuolation on H&E and marked fibrotic changes throughout the heart, with increased periostin (Figure 2C) and trichrome staining (data not shown). Although not statistically significant due to sample size, histopathologic scoring of H&E vacuolation, trichrome fibrosis, and periostin IHC staining suggested a dose-dependent increase in cardiotoxicity (Figure 2D).

As Echo is the current gold standard for detecting anthracycline-induced cardiotoxicity in pediatric patients, we aimed to correlate our histologic findings with mouse Echos. Specifically, we looked at left ventricular EF and FS, measurements currently used to clinically diagnose anthracycline cardiotoxicity [4]. Additionally, we measured E/A ratio, which is used to detect left ventricular diastolic dysfunction. Overall, we observed a variable range of echo results. No statistical significance was identified; however, there was a trend toward a reduced EF, FS, and E/A ratio in mice receiving either 20 or 30 mg/kg of Doxo (Figure 2E). In conclusion, doses of 20–30 mg/kg Doxo reproducibly induced histologic evidence of cardiotoxicity in a C57BL/6J mouse model, but there were no reproducible functional changes by echo.

3.3 | Acla Is Safe to Deliver After Doxo

After confirming that 20–30 mg/kg Doxo induces histologic evidence of cardiotoxicity, we tested the safety of Acla following Doxo exposure to model relapse treatment, hypothesizing improved tolerance due to minimal genotoxic stress. Notably, Acla dosing per cycle in the most commonly used CAG regimen in elderly AML patients in Asia is 40 mg/m^2–56 mg/m^2/cycle [25]. This is comparable to Doxo dosing per cycle as used in hematologic malignancies. Mice were treated with 5 mg/kg Doxo weekly for a total of four doses (total cumulative 20 mg/kg). After a 4-week rest period, mice were randomly assigned to receive four additional doses of 5 mg/kg Doxo (Doxo–Doxo) ($n = 15$), 5 mg/kg Acla (Doxo–Acla) ($n = 15$), or saline (Doxo–saline) ($n = 10$) weekly (additional total cumulative dose of 20 mg/kg). Mice were observed for up to 12 weeks after completion of the second course of therapy or humanely euthanized if they exhibited >15% weight loss or other significant toxicities (Figure 3A). As expected, the second course of Doxo was found to be highly toxic to the mice. Only 20% of mice were alive at study endpoint (3/15), and the group showed a median survival of 12 weeks from first dose of Doxo. This is in comparison to the Doxo–saline group, where 50% of the mice were alive at study endpoint (5/10), with a median survival of 20.5 weeks. Strikingly, the Doxo–Acla group showed the least evidence of toxicity, and 73% of mice were alive (11/15) at study endpoint, with an undefined median survival. Although the survival of the Doxo–Saline group relative to Doxo–Doxo was superior, it did not meet statistical significance ($p = 0.070$). However, as compared to the Doxo–Acla group, there was a significantly higher rate of toxic mortality in the Doxo–Doxo group ($p = 0.0098$) (Figure 3B). There was no statistical significance in the rate of toxic mortality between the Doxo–Acla group and the Doxo–Saline group ($p = 0.33$). Notably, all mice requiring humane euthanasia prior to study endpoint in the Doxo–Saline and Doxo–Acla cohorts occurred secondary to a >15% weight loss, with necropsy revealing no evidence of treatment-related toxicity.

Striking changes to baseline weights further reflect the significant differences in morbidity. All mice lost weight after the first Doxo course (Week 4) but recovered by Week 8, prior to the second course of treatment (Figure 3C). However, only the Doxo–Doxo group experienced statistically significant severe weight loss during and after the second course of therapy (Figure 3C,D). The few surviving mice in the Doxo–Doxo group largely failed to gain weight, which was not observed in the Doxo–Acla or Doxo–Saline groups. Our findings demonstrate that Acla is safe following Doxo and suggest that Acla delivery after Doxo may not increase toxic mortality.

3.4 | Accumulation of Cardiac Toxicity Is Not Observed With Acla

Given the striking increase in toxic mortality seen in the Doxo–Doxo group, we hypothesized this was secondary to cardiotoxicity. We first evaluated for histologic changes in the heart. Represen-

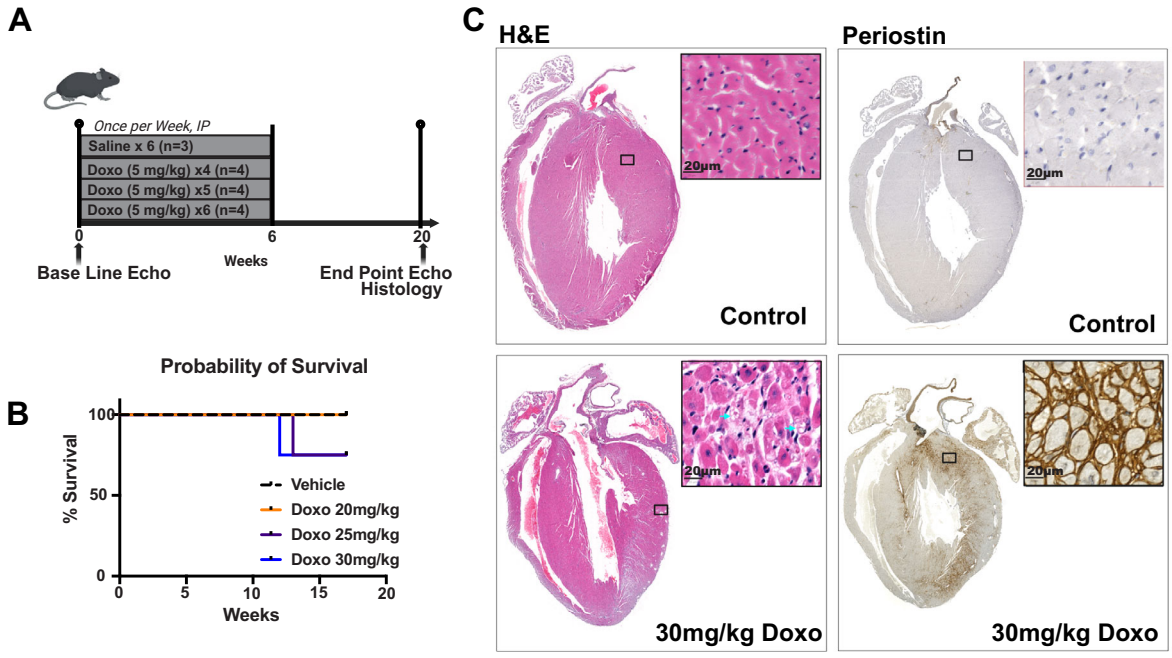

D

H&E Vacuolation		Trichrome Fibrosis		Periostin IHC Staining	
0	None observed	0	None observed	0	None observed
1	1-2 vacuolated myofibers/20X	1	1 focus/20X	1	1 focus/20X
2	3-4 vacuolated myofibers/20X	2	2 foci/20X	2	2 foci/20X
3	≥5 vacuolated myofibers/20X	3	3+ foci/20X	3	3+ foci/20X

Scoring sample sheet for an individual heart

	Score		
Heart Area	H&E	Trichrome	Periostin
Left Ventricle	0-3	0-3	0-3
Right Ventricle	0-3	0-3	0-3
Interventricular septum	0-3	0-3	0-3
Total score	0-9	0-9	0-9

Treatment Group	H&E Score
Saline (n=2)	0.0 ± 0
Doxo 20mg/kg (n=3)	2.33 ± 0.33
Doxo 25mg/kg (n=3)	3.67 ± 1.76
Doxo 30mg/kg (n=3)	4.67 ± 1.2
Treatment Group	**Periostin Score**
Saline (n=2)	0.0 ± 0
Doxo 20mg/kg (n=3)	1.33 ± 0.33
Doxo 25mg/kg (n=3)	2.33 ± 1.33
Doxo 30mg/kg (n=3)	4.33 ± 2.03
Treatment Group	**Trichrome Score**
Saline (n=2)	0.0 ± 0
Doxo 20mg/kg (n=3)	2.0 ± 0
Doxo 25mg/kg (n=3)	2.33 ± 0.88
Doxo 30mg/kg (n=3)	4.0 ± 0.58

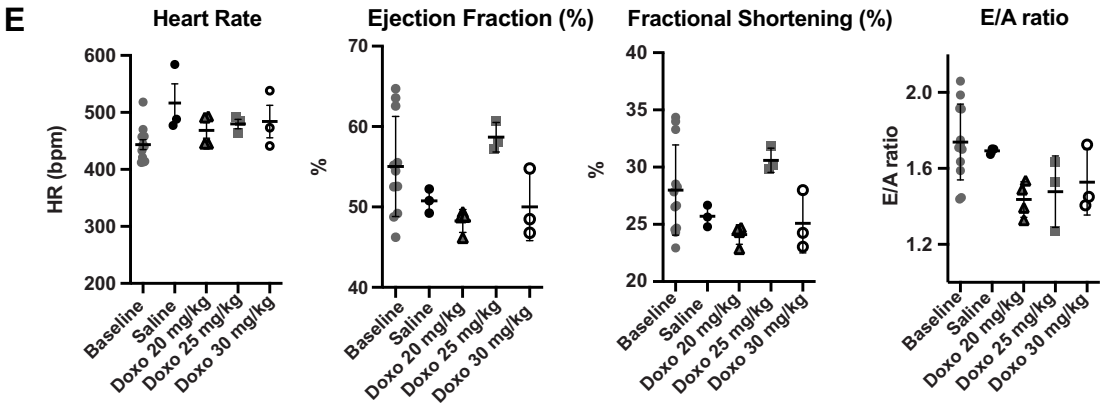

FIGURE 2 | Modeling doxorubicin cardiotoxicity in vivo. (A) Schema of xenograft study in C57BL/6J mice treated with dose escalation of Doxo. (B) Kaplan–Meier overall survival curves of individual treatment groups. (C) H&E and periostin staining of whole heart scans with magnification of blue boxed region. Blue arrow indicates areas of vacuolization. Representative images are from animals treated with total cumulative 30 mg/kg or saline. (D) Histology scoring system for H&E, trichrome, and periostin, and sample scoring sheet for an individual heart. Histology scores from H&E, trichrome, and periostin by treatment groups (mean ± SD). There was no statistical significance between treatment groups. (E) Scatter plots of echocardiogram measurements of the left ventricle and mitral valve at baseline, saline, and treatment groups (mean ± SEM). Reference ranges: HR—400–550 beats per minute; EF—47%–70%; FS—24%–40%. No statistical significance between groups. Doxo, doxorubicin; H&E, hematoxylin and eosin; IHC, immunohistochemistry; IP, intraperitoneal.

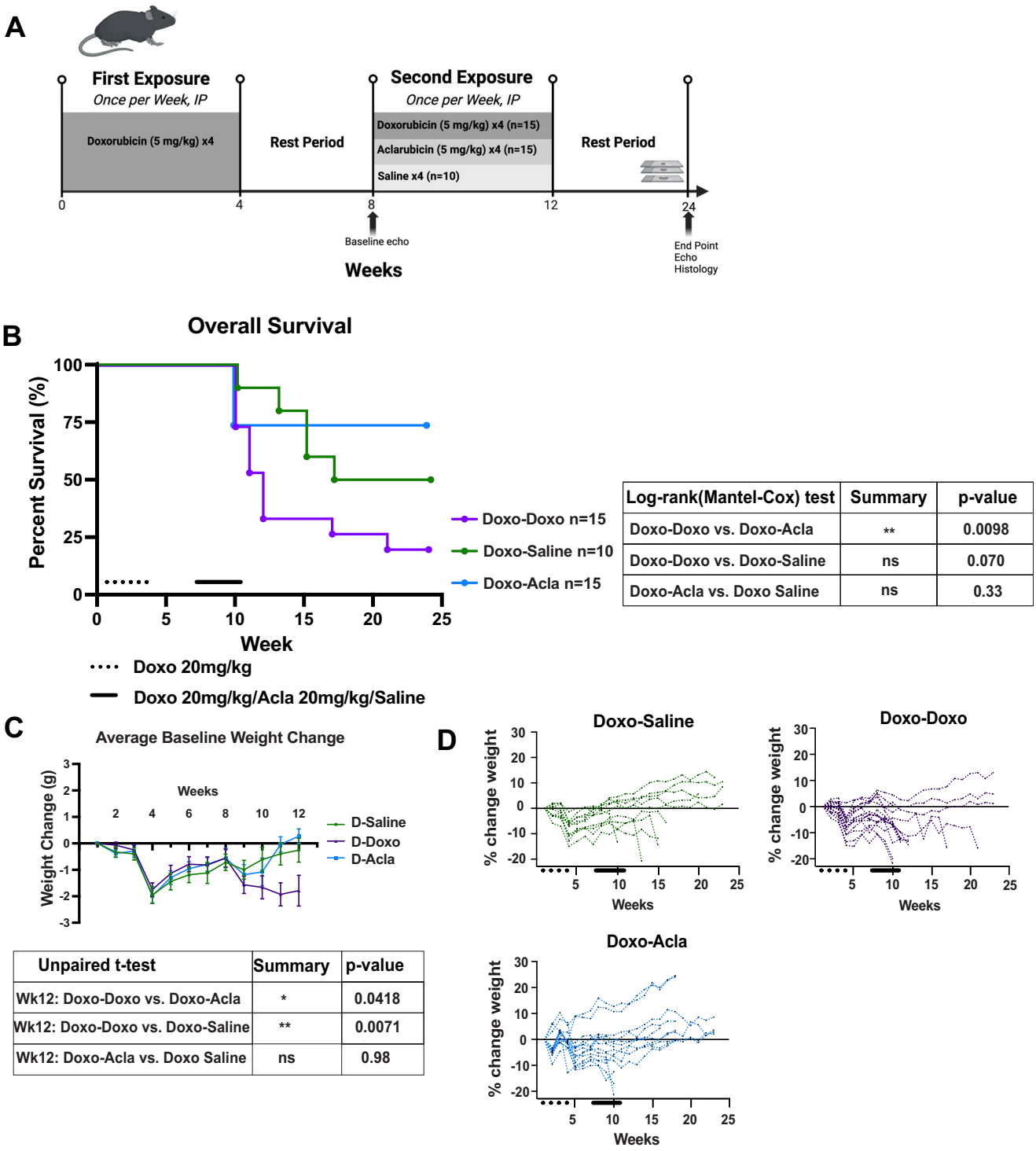

Log-rank(Mantel-Cox) test	Summary	p-value
Doxo-Doxo vs. Doxo-Acla	**	0.0098
Doxo-Doxo vs. Doxo-Saline	ns	0.070
Doxo-Acla vs. Doxo Saline	ns	0.33

Unpaired t-test	Summary	p-value
Wk12: Doxo-Doxo vs. Doxo-Acla	*	0.0418
Wk12: Doxo-Doxo vs. Doxo-Saline	**	0.0071
Wk12: Doxo-Acla vs. Doxo Saline	ns	0.98

FIGURE 3 | Aclarubicin is safe to deliver after doxorubicin. (A) Schema of xenograft study in C57BL/6J mice treated with 20 mg/kg of Acla, 20 mg/kg of Doxo, or saline after an initial 20 mg/kg of Doxo treatment. (B) Kaplan–Meier overall survival curves of individual treatment groups demonstrate a statistically significant increased toxic mortality in only mice that receive a second course of doxorubicin. Statistical significance was measured by log-rank test, with table of *p* values. (C) Change in weight (g) from baseline of each individual treatment group from weeks 1 to 12. The Doxo–Doxo treatment group had a statistically significant weight loss as compared to Doxo–Acla or Doxo–Saline group at Week 12, at the completion of the second course of treatment. Statistical significance was calculated using multiple Student *t*-test (*$p < 0.05$, **$p < 0.01$ ***$p < 0.001$). (D) Individual percentage change in weight from baseline until endpoint. Acla, aclarubicin; Doxo, doxorubicin; IP, intraperitoneal.

tative H&E and trichrome images from one mouse from each treatment group are shown in Figure 4A. Histopathologic review was performed for all mice, but scoring of H&E vacuolation (Doxo–Saline, $n = 4$; Doxo–Doxo, $n = 9$; Doxo–Acla, $n = 3$) and trichrome (Doxo–Saline, $n = 9$; Doxo–Doxo, $n = 13$; Doxo–Acla, $n = 13$) fibrosis was performed in a representative subset of mice (Figure 4B). Vacuolation and fibrosis, evidenced by increased trichrome staining, were observed across all treatment groups, as expected given that these mice had received 20 mg/kg of Doxo. Unexpectedly, despite a higher mortality, increased vacuolation and fibrosis were not seen in the Doxo–Doxo group (Figure 4C).

Next, we performed echos on 19 mice (Doxo–Doxo $n = 7$, Doxo–saline $n = 7$, Doxo–Acla $n = 5$) that were randomly selected prior to initiation of the second course of therapy. Baseline cardiac function was performed at Week 7 prior to the second course of anthracyclines. Baseline echos showed high inter-mouse variability in all cardiac measurements—EF, FS, HR, and E/A (Figure 4D). Treatment endpoint echos demonstrated no significant changes across treatment groups (Figure 4E). All mice followed by Echo in the Doxo–Acla group reached study endpoint, as compared to only 3/7 mice in the Doxo–Doxo group. Echos of surviving mice in the Doxo–Acla group and early mortality Doxo–Doxo group failed to identify significant differences (Figure 4F). Thus, despite a significantly higher rate of early toxic mortality in the Doxo–Doxo group, there was no definite histologic or echocardiographic evidence of augmented cardiotoxicity.

3.5 | End-Organ Dysfunction Is Not Observed With Acla Delivery

To define other potential causes of early mortality in Doxo–Doxo mice relative to Doxo–Acla or Doxo–Saline mice, we evaluated for additional evidence of organ dysfunction, specifically bone marrow, renal, and hepatic. CBCs were obtained at time of euthanasia, and we specifically analyzed the differences between Doxo–Acla and Doxo–Saline mice that reached study endpoint versus Doxo–Doxo mice that experienced early mortality. Doxo–Doxo mice that experienced early mortality had significantly lower total white blood cells, specifically lymphocytes. No significant differences in platelets or hemoglobin were observed (Figure 5A). Comprehensive metabolic profiles were obtained from mice that reached study endpoint from all three groups. Doxo–Doxo survivors had lower total calcium and phosphorous than Doxo–Acla survivors, and no differences in potassium levels were observed (Figure 5B). Both Doxo–Doxo and Doxo–Acla survivors had higher alanine aminotransferase (ALT) levels as compared to Doxo–Saline survivors; however, these values remained within the normal reference range (ALT: 18–94 U/L). We observed no difference in total serum bilirubin levels (Figure 5C). Finally, as measured by BUN and creatinine, no differences in renal function were observed (Figure 5D). In summary, by both necropsy and serum analysis, our studies did not detect significant end-organ damage amongst the survivors in the Doxo–Acla group, despite a cumulative anthracycline dose of 40 mg/kg. In contrast, Doxo–Doxo mice with the same dose experienced significant early mortality, though the cause was unclear both at necropsy and by serum analysis.

4 | Discussion

Anthracyclines are one of the most important classes of chemotherapy agents; however, their use is limited by cumulative dose-dependent toxicities. Acla, which induces chromatin damage without significant DNA damage, offers a promising alternative [8–11]. Our data demonstrate that Acla exhibits anti-tumor efficacy comparable to Doxo across multiple pediatric in vitro models, independent of DNA damage. Further, in vivo models recapitulating the delivery of anthracyclines after Doxo exposure, demonstrate the superior safety profile of Acla. In vivo, Acla administered after prior Doxo exposure did not exacerbate toxicity, unlike additional Doxo, which led to increased toxic mortality.

Pediatric malignancies are characterized by widespread epigenetic dysregulation, with the highest rate of mutations occurring in epigenetic regulators [26–29]. Malignancies without these mutations still demonstrate widespread epigenetic disruption, such as EwS [30, 31]. We speculate that the superior efficacy of anthracyclines in pediatric cancers may indeed stem from their ability to disrupt epigenetic programs. Interestingly, a small case series from Japan demonstrated activity of cisplatin and Acla in intracranial alveolar rhabdomyosarcoma [32]. Our studies, which demonstrate equivalent efficacy of Acla to Doxo and superior efficacy to etoposide, further support the activity of Acla in pediatric malignancies. Further validation of Acla's efficacy in mouse xenograft studies is ongoing.

Survival rates for pediatric malignancies have drastically improved. However, treatment-related toxicities, linked to anthracycline exposure, such as, cardiovascular disease and secondary malignancies, including breast cancer independent of radiation [33], are increasing in survivors [4, 34–36]. Our studies highlight the need to develop preclinical models that reproducibly model anthracycline-induced toxicities. Previous reports demonstrate a wide range of time for detection of chronic cardiac changes, anywhere between 4- and 13 weeks post-exposure [22–24, 37]. Our findings support that histologic evidence of chronic cardiac changes takes time to develop. As we initially hypothesized that a second course of Doxo would exacerbate cardiac changes, we were surprised that despite increased toxic mortality in the Doxo–Doxo group (Figure 3), cardiotoxicity was not the cause. This was likely due to the significantly shortened median survival for the Doxo–Doxo group, only 12 weeks, or 2 weeks after the final dose. As our initial analyses revealed evidence of cardiac remodeling 12 weeks after the final dose of Doxo (Figure 2), results from both models strongly support that histologic changes of cardiac remodeling require more than 8–10 weeks to manifest.

The improved survival observed in the Doxo–Acla cohort underscores the relative safety of Acla administration following prior Doxo exposure. Strikingly, the absence of cardiotoxicity in the Doxo–Doxo cohort, a well-established dose-dependent toxicity, suggests that our model captured acute rather than chronic toxicity. One mechanism of acute anthracycline toxicity is driven by systemic inflammation [38]. Doxo has been shown to activate the innate immune system, in particular Toll-like receptor 4 (TLR4), JAK/STAT signaling pathway, and inflammatory cytokines, leading to multiorgan damage and potentiating cardiac

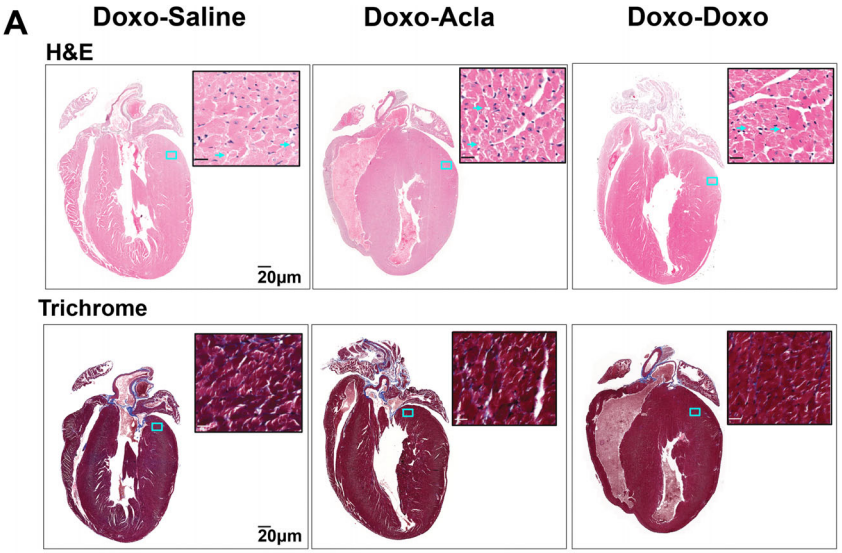

B

Histology scoring system

H&E Vacuolation		Trichrome Fibrosis	
0	None observed	0	None observed
1	Rare	1	Rare
2	<1/3 of area	2	<1/3 of area
3	1/3-2/3 of area	3	1/3-2/3 of area
4	>2/3 of area	4	>2/3 of area

Scoring sample sheet

Heart Area	Score	
	H&E	Trichrome
Left Ventricle	0-4	0-4
Right Ventricle	0-4	0-4
Interventricular septum	0-4	0-4
Total score	0-12	0-12

C

Treatment Group	H&E Score
D-S (n=4)	7.0 ± 1.4
D-D (n=9)	7.55 ± 2.45
D-A (n=3)	8.6 ± 1.33

Treatment Group	Trichrome Score
D-S (n=9)	0.77 ± 0.46
D-D (n=13)	0.46 ± 0.51
D-A (n=13)	0.38 ± 0.50

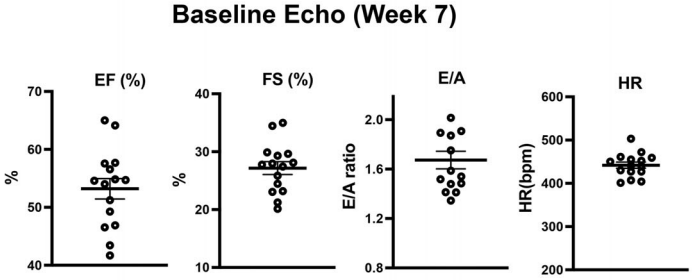

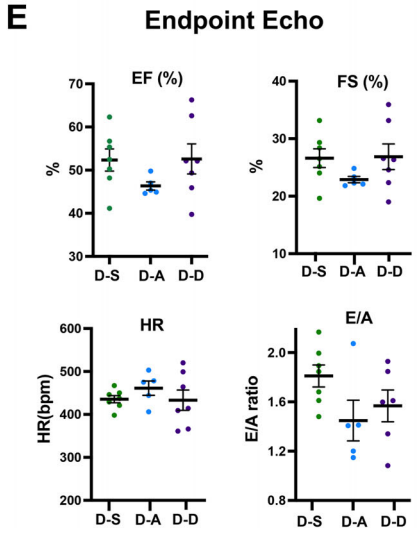

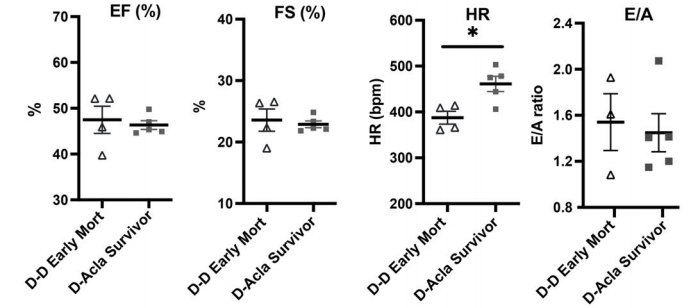

FIGURE 4 | Accumulation of significant cardiac toxicity is not observed with aclarubicin. (A) H&E and trichrome staining of whole heart scans with magnification of blue boxed region. Blue arrows indicate areas of vacuolization. Representative images are from animals at endpoint in each individual treatment group. (B) Histology scoring system for H&E and trichrome, and sample scoring sheet for an individual heart. (C) Histology scores from H&E and trichrome by treatment groups at endpoint (mean ± SD). There was no statistical significance between treatment groups. Scatter plots of echocardiogram measurements of the left ventricle and mitral valve at (D) baseline (Week 7) prior to mice receiving a second course of anthracyclines or saline, (E) at study endpoint or time of humane euthanasia, and (F) between Doxo–Doxo animals that experienced early mortality and Doxo–Acla mice that reached study endpoint. Reference range: HR—400–550 beats per minute; EF—47%–70%; FS—24%–40%. Mean ± SEM is plotted, and statistical significance was calculated using Student's *t*-test that did not show any statistical significance between groups. Acla, aclarubicin; Doxo, doxorubicin; EF, ejection fraction; FS, fractional shortening; H&E, hematoxylin and eosin; HR, heart rate; D-S, Doxo-saline; D-A, Doxo-Acla; D-D, Doxo-Doxo.

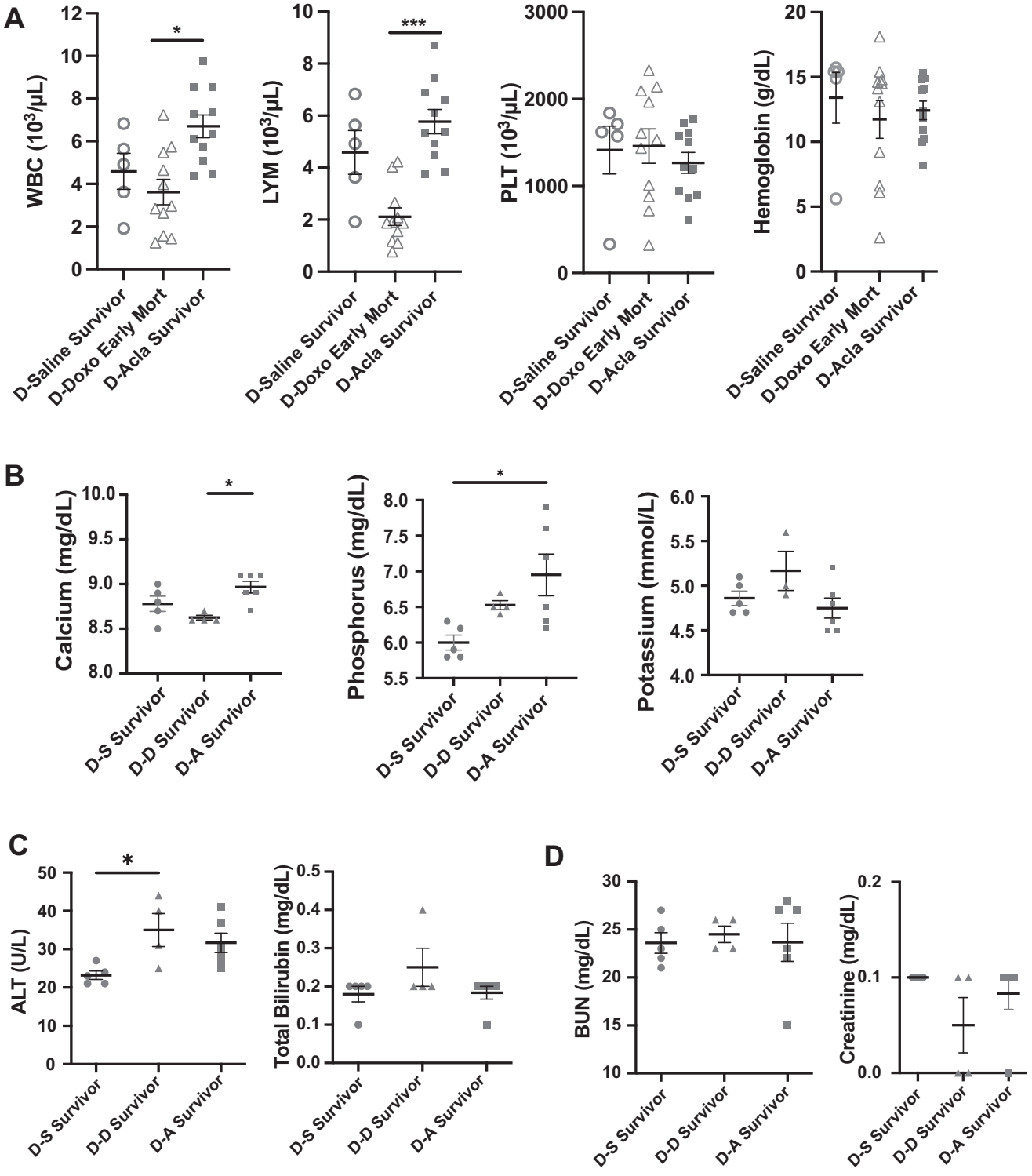

FIGURE 5 | End-organ dysfunction is not observed with aclarubicin delivery. (A) Scatter plots of complete blood count measurements of Doxo–Doxo mice that experienced early mortality and Doxo–Acla and Doxo–Saline mice that reached study endpoint. Reference range: WBC: 3.5 × 10^3/μL–6.9 × ×10^3/μL; lymphocytes: 2.92 × 10^3/μL–5.86 × ×10^3/μL; platelets 727 × 10^3/μL–1177 × 10^3/μL; hemoglobin: 10.7–12.3g/dL. Scatter plots of (B) electrolytes, (C) liver function tests, and (D) kidney function analysis of each individual treatment group of animals that reached study endpoint and did not experience early mortality. Reference range: calcium: 8.8–9.2 mg/dL; phosphorous 6.1–7.5 mg/dL; potassium: 3.8–4.2 mmol/L; ALT 18–94 U/L; total bilirubin 0.3–0.7 mg/dL; BUN 21.8–32.38 mg/dL; creatinine 0.1–0.15 mg/dL. Mean ± SEM was plotted, and statistical significance was calculated using multiple Student's *t*-test. ALT, alanine aminotransferase; Doxo, doxorubicin.

changes [38–40]. Interestingly, recent preclinical studies report that Acla can suppress these same inflammatory pathways [41]. Our observation of improved, but not statistically significant, survival in the Doxo–Acla group as compared to the Doxo–Saline group suggests that Acla may even exert a protective effect, potentially by mitigating inflammatory responses. Validation of this differential inflammatory response in our model will be important to demonstrate in future experiments.

Notable limitations of our study include the small sample size in the Doxo–saline group, due to unexpected premature mortality of unclear etiology, which reduced statistical power and limited comparisons with the Doxo–Acla and Doxo–Doxo cohorts. In addition, only a small number of mice underwent echocardiography, particularly among those with early mortality, constraining our ability to assess cardiac function across cohorts. Finally, because our model more closely reflects acute rather than chronic anthracycline toxicity, histologic changes in the hearts of mice that experienced early mortality may not have been captured.

Future studies will focus on validating our in vitro efficacy results in in vivo xenograft models. Confirmation of potent anti-tumor activity in these models, together with the favorable safety profile of Acla, will establish the foundation for advancing Acla towards clinical translation. We anticipate proposing the incorporation of Acla into relapsed/refractory regimens, particularly in combination with other novel agents, an approach already employed in Asia for adult AML patients with encouraging efficacy and a favorable safety profile [12, 25]. In summary, our results demonstrate that Acla has potent anti-tumor activity across multiple pediatric malignancies while exhibiting a superior safety profile, enabling its use following prior Doxo exposure. These findings highlight the potential of Acla in pediatric cancer therapy and support its further clinical investigation.

Acknowledgments

The authors thank members of the Lawlor, Sarthy, Neefjes, Olson, and Maves labs for helpful discussions and the staff at the Seattle Children's Research Institute histology and microscopy core and animal core. We would also like to thank colleagues at University of Washington, Department of Veterinary Medicine. Grant and gift support for this work is gratefully acknowledged and was provided by the following sources: NIH/NCI 5K12CA076930 (SSG), NIH/NCI Loan Repayment Grant 1L40CA264716 (SSG), CURE Childhood Cancer (SSG, ERL, JFS), Sam Day Foundation (LM, ERL, JFS), Burroughs Wellcome Fund (JFS), Andy Hill CARE Fund (JFS), Sunbeam Foundation (JFS), NIH/NCI 5K08CA256167 (JFS), and NIH/NCI 1R21CA280139 (LM, ERL, AO).

Conflicts of Interest

Dr. Jacques Neefjes is a shareholder in NIHM that aims to produce aclarubicin for clinical use. The authors declare no conflicts of interest.

References

1. Y. Wang, C. M. Ronckers, F. E. van Leeuwen, et al., "Subsequent Female Breast Cancer Risk Associated With Anthracycline Chemotherapy for Childhood Cancer," *Nature Medicine* 29, no. 9 (2023): 2268–2277, https://doi.org/10.1038/s41591-023-02514-1.

2. J. M. Yeh, Z. J. Ward, A. Chaudhry, et al., "Life Expectancy of Adult Survivors of Childhood Cancer Over 3 Decades," *JAMA Oncology* 6, no. 3 (2020): 350–357, https://doi.org/10.1001/jamaoncol.2019.5582.

3. A. T. Meadows, D. L. Friedman, J. P. Neglia, et al., "Second Neoplasms in Survivors of Childhood Cancer: Findings From the Childhood Cancer Survivor Study Cohort," *Journal of Clinical Oncology* 27, no. 14 (2009): 2356–2362, https://doi.org/10.1200/JCO.2008.21.1920.

4. S. Bhatia, "Genetics of Anthracycline Cardiomyopathy in Cancer Survivors: JACC: CardioOncology State-of-the-Art Review," *JACC CardioOncology* 2, no. 4 (2020): 539–552, https://doi.org/10.1016/j.jaccao.2020.09.006.

5. K. M. Tewey, T. C. Rowe, L. Yang, B. D. Halligan, and L. F. Liu, "Adriamycin-Induced DNA Damage Mediated by Mammalian DNA Topoisomerase II," *Science* 226, no. 4673 (1984): 466–468, https://doi.org/10.1126/science.6093249.

6. S. Zhang, X. Liu, T. Bawa-Khalfe, et al., "Identification of the Molecular Basis of Doxorubicin-Induced Cardiotoxicity," *Nature Medicine* 18, no. 11 (2012): 1639–1642, https://doi.org/10.1038/nm.2919.

7. E. H. Herman, J. Zhang, B. B. Hasinoff, J. R. Clark Jr., and V. J. Ferrans, "Comparison of the Structural Changes Induced by Doxorubicin and Mitoxantrone in the Heart, Kidney and Intestine and Characterization of the Fe(III)-Mitoxantrone Complex," *Journal of Molecular and Cellular Cardiology* 29, no. 9 (1997): 2415–2430, https://doi.org/10.1006/jmcc.1997.0477.

8. B. Pang, X. Qiao, L. Janssen, et al., "Drug-Induced Histone Eviction From Open Chromatin Contributes to the Chemotherapeutic Effects of Doxorubicin," *Nature Communications* 4 (2013): 1908, https://doi.org/10.1038/ncomms2921.

9. F. Yang, C. J. Kemp, and S. Henikoff, "Doxorubicin Enhances Nucleosome Turnover Around Promoters," *Current Biology* 23, no. 9 (2013): 782–787, https://doi.org/10.1016/j.cub.2013.03.043.

10. E. Nesher, A. Safina, I. Aljahdali, et al., "Role of Chromatin Damage and Chromatin Trapping of FACT in Mediating the Anticancer Cytotoxicity of DNA-Binding Small-Molecule Drugs," *Cancer Research* 78, no. 6 (2018): 1431–1443, https://doi.org/10.1158/0008-5472.CAN-17-2690.

11. S. Y. van der Zanden, X. Qiao, and J. Neefjes, "New Insights Into the Activities and Toxicities of the Old Anticancer Drug Doxorubicin," *FEBS Journal* 288, no. 21 (2021): 6095–6111, https://doi.org/10.1111/febs.15583.

12. X. Qiao, S. Y. van der Zanden, and X. Li, "Diversifying the Anthracycline Class of Anti-Cancer Drugs Identifies Aclarubicin for Superior Survival of Acute Myeloid Leukemia Patients," *Molecular Cancer* 23, no. 1 (2024): 120, https://doi.org/10.1186/s12943-024-02034-7.

13. X. Qiao, S. Y. van der Zanden, and D. P. A. Wander, "Uncoupling DNA Damage From Chromatin Damage to Detoxify Doxorubicin," *PNAS* 117, no. 26 (2020): 15182–15192, https://doi.org/10.1073/pnas.1922072117.

14. J. Neefjes, K. Gurova, J. Sarthy, G. Szabo, and S. Henikoff, "Chromatin as an Old and New Anticancer Target," *Trends in Cancer* 10, no. 8 (2024): 696–707, https://doi.org/10.1016/j.trecan.2024.05.005.

15. K. Saito, Y. Nakamura, M. Aoyagi, et al., "Low-Dose Cytarabine and Aclarubicin in Combination With Granulocyte Colony-Stimulating Factor (CAG Regimen) for Previously Treated Patients With Relapsed or Primary Resistant Acute Myelogenous Leukemia (AML) and Previously Untreated Elderly Patients With AML, Secondary AML, and Refractory Anemia With Excess Blasts in Transformation," *International Journal of Hematology* 71, no. 3 (2000): 238–244.

16. H. H. Zhu, H. Jiang, B. Jiang, et al., "Cytarabine, Aclarubicin and Granulocyte Colony-Stimulating Factor Regimen Represents an Effective and Safe Salvage Regimen for Patients With Acute Myeloid Leukemia Refractory to First Course of Induction Chemotherapy," *Leukemia & Lymphoma* 54, no. 11 (2013): 2452–2457, https://doi.org/10.3109/10428194.2013.776679.

17. W. Kern, J. Braess, A. Grote-Metke, et al., "Combination of Aclarubicin and Etoposide for the Treatment of Advanced Acute Myeloid Leukemia:

Results of a Prospective Multicenter Phase II Trial. German AML Cooperative Group," *Leukemia* 12, no. 10 (1998): 1522–1526, https://doi.org/10.1038/sj.leu.2401155.

18. National Research Council (U.S.), Committee for the Update of the Guide for the Care and Use of Laboratory Animals, Institute for Laboratory Animal Research (U.S.), National Academies Press (U.S.), *Guide for the Care and Use of Laboratory Animals*, 8th ed. (National Academies Press, 2011), http://www.ncbi.nlm.nih.gov/books/NBK54050.

19. A. K. Olson, D. Ledee, K. Iwamoto, et al., "C-Myc Induced Compensated Cardiac Hypertrophy Increases Free Fatty Acid Utilization for the Citric Acid Cycle," *Journal of Molecular and Cellular Cardiology* 55 (2013): 156–164, https://doi.org/10.1016/j.yjmcc.2012.07.005.

20. W. Z. Zhu, T. Palazzo, M. Zhou, et al., "First Comprehensive Identification of Cardiac Proteins With Putative Increased O-GlcNAc Levels During Pressure Overload Hypertrophy," *PLoS ONE* 17, no. 10 (2022): e0276285, https://doi.org/10.1371/journal.pone.0276285.

21. Q. A. J. Hagdorn, G. P. L. Bossers, A. C. Koop, et al., "A Novel Method Optimizing the Normalization of Cardiac Parameters in Small Animal Models: The Importance of Dimensional Indexing," *American Journal of Physiology. Heart and Circulatory Physiology* 316, no. 6 (2019): H1552–H1557, https://doi.org/10.1152/ajpheart.00182.2019.

22. C. S. Abdullah, S. Alam, R. Aishwarya, et al., "Doxorubicin-Induced Cardiomyopathy Associated With Inhibition of Autophagic Degradation Process and Defects in Mitochondrial Respiration," *Scientific Reports* 9, no. 1 (2019): 2002, https://doi.org/10.1038/s41598-018-37862-3.

23. R. Hullin, M. Metrich, A. Sarre, et al., "Diverging Effects of Enalapril or Eplerenone in Primary Prevention Against Doxorubicin-Induced Cardiotoxicity," *Cardiovascular Research* 114, no. 2 (2018): 272–281, https://doi.org/10.1093/cvr/cvx162.

24. C. J. Zeiss, D. M. Gatti, O. Toro-Salazar, et al., "Doxorubicin-Induced Cardiotoxicity in Collaborative Cross (CC) Mice Recapitulates Individual Cardiotoxicity in Humans," *G3 Genes|Genomes|Genetics* 9, no. 8 (2019): 2637–2646, https://doi.org/10.1534/g3.119.400232.

25. G. Wei, W. Ni, J. W. Chiao, Z. Cai, H. Huang, and D. Liu, "A Meta-Analysis of CAG (Cytarabine, Aclarubicin, G-CSF) Regimen for the Treatment of 1029 Patients With Acute Myeloid Leukemia and Myelodysplastic Syndrome," *Journal of Hematology & Oncology* 4 (2011): 46, https://doi.org/10.1186/1756-8722-4-46.

26. E. Panditharatna and M. G. Filbin, "The Growing Role of Epigenetics in Childhood Cancers," *Current Opinion in Pediatrics* 32, no. 1 (2020): 67–75, https://doi.org/10.1097/MOP.0000000000000867.

27. R. Huether, L. Dong, X. Chen, et al., "The Landscape of Somatic Mutations in Epigenetic Regulators Across 1,000 Paediatric Cancer Genomes," *Nature Communications* 5 (2014): 3630, https://doi.org/10.1038/ncomms4630.

28. E. R. Lawlor and C. J. Thiele, "Epigenetic Changes in Pediatric Solid Tumors: Promising New Targets," *Clinical Cancer Research* 18, no. 10 (2012): 2768–2779, https://doi.org/10.1158/1078-0432.CCR-11-1921.

29. S. N. Grobner, B. C. Worst, J. Weischenfeldt, et al., "The Landscape of Genomic Alterations Across Childhood Cancers," *Nature* 555, no. 7696 (2018): 321–327, https://doi.org/10.1038/nature25480.

30. N. Riggi, B. Knoechel, S. M. Gillespie, et al., "EWS-FLI1 Utilizes Divergent Chromatin Remodeling Mechanisms to Directly Activate or Repress Enhancer Elements in Ewing Sarcoma," *Cancer Cell* 26, no. 5 (2014): 668–681, https://doi.org/10.1016/j.ccell.2014.10.004.

31. G. Boulay, G. J. Sandoval, N. Riggi, et al., "Cancer-Specific Retargeting of BAF Complexes by a Prion-Like Domain," *Cell* 171, no. 1 (2017): 163–178 e19, https://doi.org/10.1016/j.cell.2017.07.036.

32. T. Wakabayashi, J. Yoshida, J. Ishiyama, and N. Kageyama, "Clinical Trials of Combination Chemotherapy Using Cis-Platinum With Aclarubicin in Intracranial Rhabdomyosarcoma," *Gan to Kagaku Ryoho Cancer & Chemotherapy* 14, no. 7 (1987): 2374–2377.

33. T. O. Henderson, C. S. Moskowitz, J. F. Chou, et al., "Breast Cancer Risk in Childhood Cancer Survivors Without a History of Chest Radiotherapy: A Report From the Childhood Cancer Survivor Study," *Journal of Clinical Oncology* 34, no. 9 (2016): 910–918, https://doi.org/10.1200/JCO.2015.62.3314.

34. N. Bhakta, Q. Liu, K. K. Ness, et al., "The Cumulative Burden of Surviving Childhood Cancer: An Initial Report From the St Jude Lifetime Cohort Study (SJLIFE)," *Lancet* 390, no. 10112 (2017): 2569–2582, https://doi.org/10.1016/S0140-6736(17)31610-0.

35. A. M. Williams, Q. Liu, N. Bhakta, et al., "Rethinking Success in Pediatric Oncology: Beyond 5-Year Survival," *Journal of Clinical Oncology* 39, no. 20 (2021): 2227–2231, https://doi.org/10.1200/JCO.20.03681.

36. E. J. Chow, K. J. Leger, N. S. Bhatt, et al., "Paediatric Cardio-Oncology: Epidemiology, Screening, Prevention, and Treatment," *Cardiovascular Research* 115, no. 5 (2019): 922–934, https://doi.org/10.1093/cvr/cvz031.

37. E. Y. Podyacheva, E. A. Kushnareva, A. A. Karpov, and Y. G. Toropova, "Analysis of Models of Doxorubicin-Induced Cardiomyopathy in Rats and Mice. A Modern View From the Perspective of the Pathophysiologist and the Clinician," *Frontiers in Pharmacology* 12 (2021): 670479, https://doi.org/10.3389/fphar.2021.670479.

38. L. Wang, Q. Chen, H. Qi, et al., "Doxorubicin-Induced Systemic Inflammation Is Driven by Upregulation of Toll-Like Receptor TLR4 and Endotoxin Leakage," *Cancer Research* 76, no. 22 (2016): 6631–6642, https://doi.org/10.1158/0008-5472.CAN-15-3034.

39. D. V. Krysko, A. Kaczmarek, O. Krysko, et al., "TLR-2 and TLR-9 Are Sensors of Apoptosis in a Mouse Model of Doxorubicin-Induced Acute Inflammation," *Cell Death and Differentiation* 18, no. 8 (2011): 1316–1325, https://doi.org/10.1038/cdd.2011.4.

40. E. Hutchins, E. H. Yang, and A. F. Stein-Merlob, "Inflammation in Chemotherapy-Induced Cardiotoxicity," *Current Cardiology Reports* 26, no. 12 (2024): 1329–1340, https://doi.org/10.1007/s11886-024-02131-5.

41. A. F. Chora, D. Pedroso, E. Kyriakou, et al., "DNA Damage Independent Inhibition of NF-kappaB Transcription by Anthracyclines," *Elife* 11 (2022): e77443, https://doi.org/10.7554/eLife.77443.